https://doi.org/10.1016/j.engstruct.2023.116892

Artificial Intelligence (AI)-Assisted Simulation-Driven Earthquake-Resistant Design Framework: Taking a Strong Back System as an Example

Chen Wang[1], Junxian Zhao[2], Tak-Ming Chan[1, *]

[1]Department of Civil and Environmental Engineering, The Hong Kong Polytechnic University, Hung Hom, Hong Kong, China.

[2]School of Civil Engineering and Transportation, South China University of Technology, Guangzhou, China

[*] Email: tak-ming.chan@polyu.edu.hk

Abstract

Traditional earthquake-resistant structural design considers only a limited number of factors, mainly elastic structural properties, to determine key design parameters. However, these parameters are often not optimal because they do not take into account the extensive plasticity expected in building structures during earthquakes. To address this issue, an artificial intelligence (AI)-assisted simulation-driven framework has been developed in this study. This framework can automatically output optimal design parameters while considering nonlinear structural response under strong earthquakes and a large number of input factors. The primary innovation of the proposed framework lies in the fusion and integration of nonlinear numerical simulation and AI tools for earthquake-resistant design of building structures, marking a promising trend in this field. The framework consists of two steps. In the first step, a database that consists of optimal design parameters and covers a wide range of design inputs will be created through numerical nonlinear response history analyses (NRHAs). In the second step, AI models will be created and trained based on the database to automatically output the optimal design parameters. To illustrate the basic components underlying the proposed framework, the determination of the height-wise distribution (denoted by $\boldsymbol{\Psi}$) of the total design lateral force for a strong back system is taken as an example. A database of 1200 samples was created

through NRHAs, and an artificial neural network (ANN) model was created, optimized, and trained. The developed ANN model yielded optimal $\boldsymbol{\Psi}$ with the majority of absolute errors within 1%, demonstrating the feasibility of our proposed AI-assisted simulation-driven earthquake-resistant design framework.

Keywords: artificial intelligence, earthquake-resistant design, nonlinear response history analyses, simulation-driven, neural network

Nomenclature

b	Bias in the relationship between two nodes in the neural network
$\boldsymbol{h}$	Story height
h_i	Story height of the i^{th} story / Output value of the i^{th} node in the hidden layer of the neural network
$K_{v,i}$	The shear stiffness of the spring for the strong back at the i^{th} story
$\boldsymbol{m}$	Seismic mass
m_i	Seismic mass of the i^{th} floor
V	Total design lateral force
$V_{y,i}$	The yield lateral resistance of the strong back at the i^{th} story
w	Weight in the relationship between two nodes in the neural network
W	Total seismic weight
$\delta_{y,i}$	The yield inter-story drift of the strong back at the i^{th} story
Δ	Step size to control the magnitude of update of $\boldsymbol{\Psi}$ in each iteration
η	The performance score (see Eq. 7)
$\theta_{y,SB}$	Yield inter-story drift ratio of the strong back
$\boldsymbol{\theta}^i_{max}$	The maximum absolute inter-story drift ratio under ground motion i
$\overline{\boldsymbol{\theta}}_{max}$	The mean of $\boldsymbol{\theta}^i_{max}$ under 22 ground motions (see Eq. 4)
ξ	Damping ratio
$\boldsymbol{\Psi}$	The distribution of V over the stories, with a sum of 1
Ψ_i	Portion of V assigned to floor level i

Note: Bold letters represent vectors while un-bold letters represent scalars.

1 Introduction

For the determination of some key design parameters in earthquake-resistant design, a limited number of factors and mainly elastic structural properties are considered in conventional methods. One typical example is the height-wise distribution of the total design lateral force, which is denoted by $\boldsymbol{\Psi}$ in this paper. In most seismic design codes, e.g., ASCE 7-16 (ASCE, 2016), Eurocode 8 (CEN, 2004), GB 50011 (2016), NBCC (NRCC, 2015), etc., $\boldsymbol{\Psi}$ is generally determined based on the elastic dynamic properties of the structure and follows the typical relationship

$$\Psi_i = \frac{m_i h_i^k}{\sum_{j=1}^{n} m_j h_j^k} \tag{1}$$

where m_i and h_i are the seismic mass and height of the i^{th} story above the base, respectively, n is the number of stories, k is an empirical factor to modify the distribution shape and varies from code to code. In some codes (e.g., NBCC (NRCC, 2015)), an additional concentrated lateral force at the top level is added to account for the higher-mode effect.

However, under design-level conditions (typically with a return period of 475 years) and stronger earthquakes, extensive plasticity is expected in building structures (Kassem et al., 2022 a & b). The effect of the code compliant $\boldsymbol{\Psi}$ has been extensively studied by various researchers (Anderson et al., 1991; Chopra, 2001; Hajirasouliha & Moghaddam, 2009; Chao et al., 2007). It was found that the code compliant $\boldsymbol{\Psi}$ may not be the optimal one especially when the structural response in the nonlinear range is considered. For instance, Chao et al. (2007) reviewed and studied the $\boldsymbol{\Psi}$ used in current seismic code through nonlinear dynamic analyses of a number of example structures. It was concluded that code lateral distributions do not represent the maximum force distribution that may be induced during nonlinear response, which may lead to inaccurate predictions of deformation and force demands, causing structures to behave in a rather unpredictable and undesirable manner. Chopra (2001) evaluated the

ductility demands of several shear-building models subjected to the El-Centro Earthquake of 1940. The yield strength distribution over stories of these models was chosen in accordance with the distribution patterns of the earthquake forces specified in the Uniform Building Code (UBC, 1997). It was concluded that this distribution pattern does not lead to equal ductility demand in all stories, and that in most cases the ductility demand in the first story is the largest of all stories.

Determining the optimal $\boldsymbol{\Psi}$ involves many factors and the nonlinear structural response that conventional design methods struggle to fully account for. On the other hand, artificial intelligence (AI) techniques have demonstrated an exceptional ability to recognize highly complex relationships between a large number of input and output parameters. AI techniques have been increasingly adopted in the fields of structural engineering and earthquake engineering. For instance, Calledda et al. (2021) recently presented a procedure combining non-linear time-history analyses with artificial neural network (ANN) training and inversion to obtain cost-effective earthquake-resistant designs for reinforced concrete buildings. The ANN approach has also been successfully employed for predicting structural responses and conducting structural optimization (Brown et al., 2005; Conte et al., 1994; Möller et al., 2009; Messner et al., 1994). Mitropoulou & Papadrakakis (2011), Jough & Sensoy (2016), and Kiani et al. (2019) have reported the application of machine learning models for predicting seismic collapse and deriving seismic fragility curves. Moreover, Xiao et al. (2022) and Wang & Chan (2023) have successfully employed various machine learning methods to predict the strengths of different structural components.

To deal with the aforementioned issue, in this paper, an AI-assisted simulation-driven earthquake-resistant design framework was developed that can automatically output optimal design parameters while considering nonlinear structural response under strong earthquakes and a large number of input factors. The concept of the proposed framework was elaborated,

and the determination of the optimal $\boldsymbol{\Psi}$ for a strong back system is used as an example to illustrate the basic components and procedures. Firstly, the strong back system is introduced and a numerical model that can capture both the elastic and plastic properties of the system is developed. An optimization algorithm was then developed and implemented to find the optimal $\boldsymbol{\Psi}$ based on numerical nonlinear response history analyses (NRHAs) under a set of ground motions. Subsequently, comprehensive parametric studies were conducted to find the optimal $\boldsymbol{\Psi}$s for a wide range of design inputs, resulting in a database of 1200 samples. An artificial neural network (ANN) model was then created, optimized, and trained based on the database. Lastly, the trained ANN model was used to output the optimal $\boldsymbol{\Psi}$s for 240 unseen design cases and its performance was evaluated accordingly.

2 Concept of the AI-assisted simulation-driven earthquake-resistant design framework

The AI-assisted simulation-driven earthquake-resistant design framework is proposed in this paper and is illustrated in Figure 1. The ultimate objective of this framework is to develop tools that can yield optimal design parameters for earthquake-resistant design of structures which take into account a large number of design input factors and nonlinear structural responses under strong earthquakes. The tools can be directly used by structural engineers for whom the structural modeling and analysis can be waived.

The framework is composed of two steps. In the first step, a large number of buildings covering a wide range of design inputs will be considered. For each building, the optimal design parameters for earthquake-resistant design will be obtained through nonlinear numerical simulations under a set of ground motion records. A database containing pairs of design inputs and optimal design parameters for earthquake-resistant design will be created. The data can be accumulated over time and the contents and size of the database will keep growing. In the second step, AI models (e.g., neural networks) will be built and trained based on the created database. When fed with the input of a new building, the developed AI models can yield the

optimal design parameters that can be used directly by structural engineers to conduct the earthquake-resistant design, and the structural modeling and analysis can be waived.

The primary innovation of the proposed framework lies in the fusion and integration of nonlinear numerical simulation and AI tools for earthquake-resistant design of building structures, marking a promising trend in this field. Each component of the proposed simulation-driven AI-assisted framework, on its own, is not novel. Instead, it is the fusion of these components, particularly the combination of nonlinear numerical simulation and AI, that showcases the true power and superiority of the proposed design method.

It is important to note that the proposed AI-assisted simulation-driven design framework is not aimed at completely replacing the current design codes. Instead, it seeks to complement the existing codes and assist engineers in identifying optimal key design parameters that surpass the specifications outlined in the codes. For capacity-based design, the proposed design procedure can be used to determine some key design parameters for the design of fuse elements, with subsequent linear elastic structural analyses performed under the designated seismic loads. Nevertheless, for the design of other structural members, an additional structural analysis is required, assuming that all the fuse elements have reached their capacity.

In the remainder of this paper, the height-wise distribution of the total design lateral force (which is denoted by $\boldsymbol{\Psi}$) for a strong back system is taken as an example to illustrate the basic components and the functionality of the proposed framework.

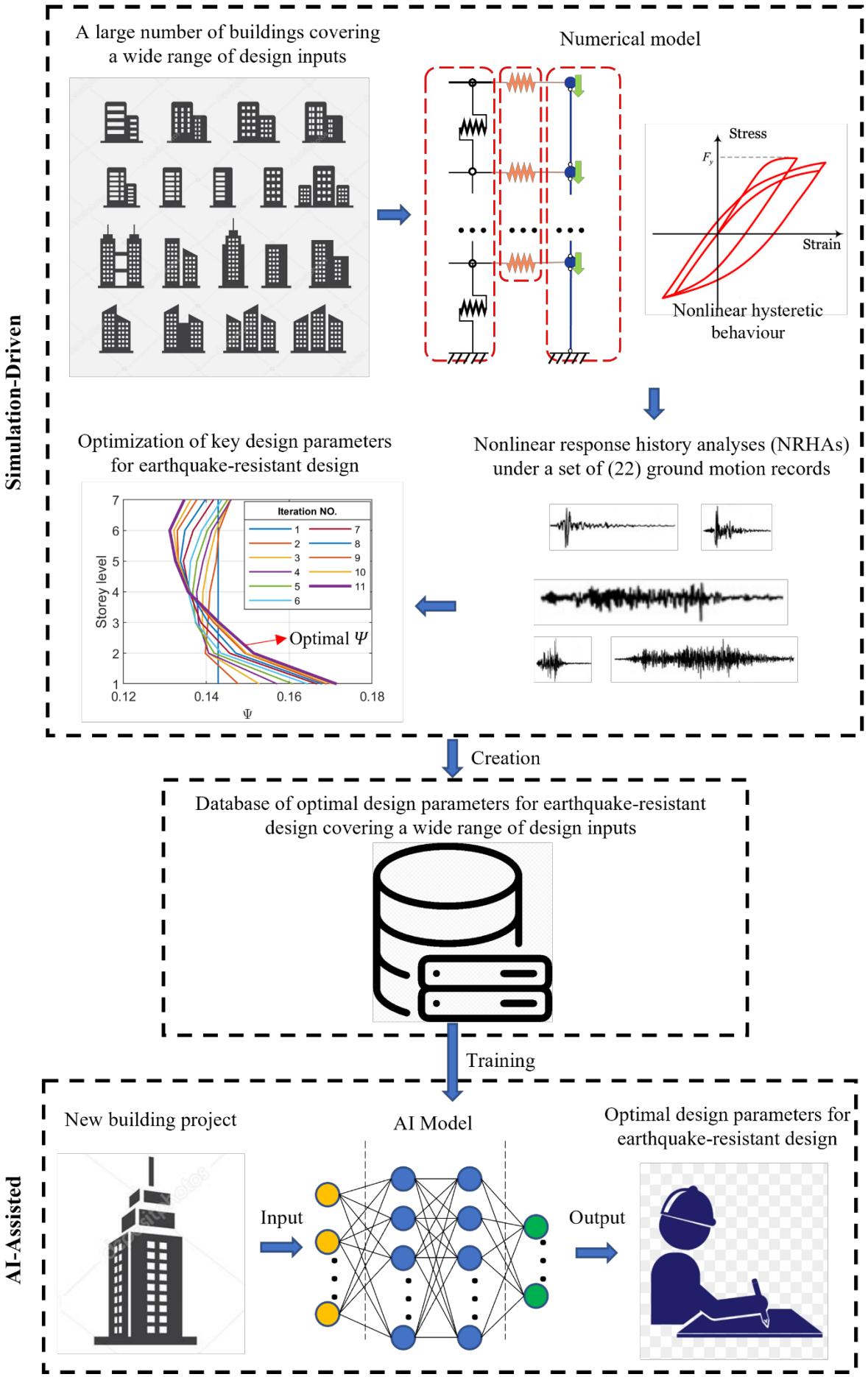
Simulation-Driven
A large number of buildings covering a wide range of design inputs
Numerical model
Stress
Strain
Nonlinear hysteretic behaviour
Optimization of key design parameters for earthquake-resistant design
Nonlinear response history analyses (NRHAs) under a set of (22) ground motion records
Iteration NO.
Storey level
Optimal Ψ
Creation
Database of optimal design parameters for earthquake-resistant design covering a wide range of design inputs
Training
AI-Assisted
New building project
AI Model
Optimal design parameters for earthquake-resistant design
Input
Output

Figure 1 Illustration of the proposed AI-assisted simulation-driven earthquake-resistant design framework

3 Introduction of the strong back system

To improve the performance of building structures under strong earthquakes, the concept of strong back has been proposed by previous researchers (Tremblay, 2003; Lai & Mahin, 2015; Takeuchi et al., 2015), in which part of the building is intentionally designed to be stronger to remain essentially elastic under strong earthquakes. In light of the previous studies, a strong back with ductile link (SBDL) system is proposed which is illustrated in Figure 2. In this system, the gravity frame is connected to the strong back via buckling-restrained braces (BRBs) which are known for their excellent energy dissipation capacity (Zhao et al., 2021, 2023). Different structures can be used as the strong back, for instance, steel braced frames, reinforced concrete walls, etc. Under strong earthquakes, the strong back is intended to remain elastic, while the energy is mainly dissipated by BRBs through plastic cyclic axial deformations.

For the design of the SBDL system, once the total design lateral force V is determined, the key design parameter is the height-wise distribution of V to different floors which is denoted by $\boldsymbol{\Psi}$. The design lateral force at the i^{th} floor, calculated as $V \cdot \Psi_i$, determines the design of BRBs at the i^{th} floor. The strong back can be subsequently designed based on the capacities of BRBs (assuming all BRBs have reached their capacities) following the capacity-based design principle.

In this paper, the determination of the optimal $\boldsymbol{\Psi}$ for the SBDL system of a 7-story building (as shown in Figure 2) is taken as an example to illustrate the basic components underlying the proposed AI-assisted simulation-driven earthquake-resistant design framework. The SBDL earthquake-resistant system for the 7-story prototype building is illustrated in Figure 3

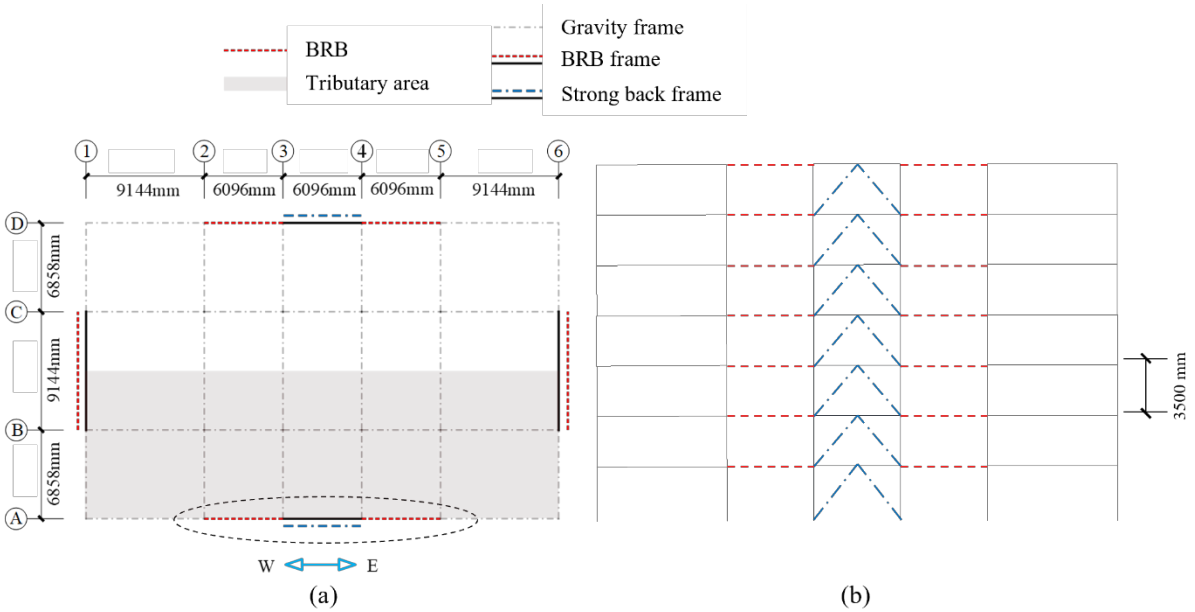

153

154 **Figure 2** Prototype building with the strong back system: (a) plan view, (b) elevation view

155

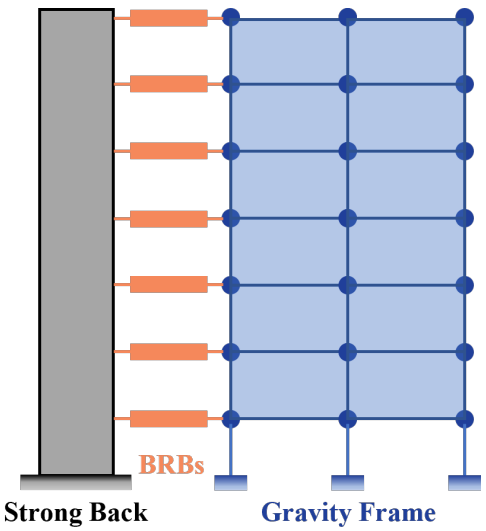

156

157 **Figure 3** Illustration of the strong back-ductile link (SBDL) system for the prototype building

158 The building was assumed to be regular in both plan and elevation planes. Therefore, the
159 three-dimensional effects are expected to be minimal under earthquake excitations and a plane
160 model was adopted in the analysis. Only earthquake excitations in the E-W directions were
161 considered. Given the symmetry of the building, minimal differential vertical movements are
162 expected, and the building's response will be primarily governed by its horizontal behavior.
163 Moreover, as the earthquake-resisting system is primarily intended to resist horizontal forces,

the vertical component of ground motion was neglected in the analysis. Some information about the prototype building is listed in Table 1. It is noted that the seismicity of the site where the building is built is quantified following the framework of ASCE 7-16 (ASCE, 2016), which will be used to select and scale the set of ground motion records as explained in Section 4.1.

Table 1 Information of the prototype building

Total seismic mass	2475 tons
BRBs	Length: 6000 mm Steel grade of core plates: ASTM A36
Seismicity parameters	Seismic Design Category (SDC): C Site class: C The design spectral response acceleration parameter at short periods S_{DS} = 0.5g The design spectral response acceleration parameter at the 1-s period S_{D1} = 0.2g

3.1 Numerical modeling of the SBDL system

A numerical model that can capture both the elastic and plastic properties of the SBDL system is developed (as shown in Figure 4) and implemented in the Open System for Earthquake Engineering Simulation (*OpenSees*) platform (McKenna et al., 2010). Firstly, the gravity frame is assumed to resist gravity only and not to provide lateral resistance. The seismic mass of the building at each floor is idealized as a concentrated mass and they are vertically connected by rigid elements with pinned ends. Gravity loads are applied to the mass nodes to account for the *P-Δ* effect. The BRBs are modeled by truss elements. The area of the truss element was set as the area of the core plate of the corresponding BRB. The *Steel02* material model (Giuffré-Menegotto-Pinto Model with isotropic strain hardening) in *OpenSees* was assigned to model the full-range (both elastic and plastic) behavior of BRBs with the

recommended parameters *R0*=15, *cR1*=0.925, *cR2*=0.15 (Mazzoni et al., 2006). For the core plate of BRBs, the steel of Grade ASTM A36 was assumed to have an expected yield strength of 320 MPa and a strain hardening ratio of 0.3%. As the plastic deformation of BRBs concentrates in the core plate which is typically 2/3 of the whole length of the BRB, the length of the truss element was set to be 2/3 of the length of the corresponding BRB (Zsarnoczay, 2003).

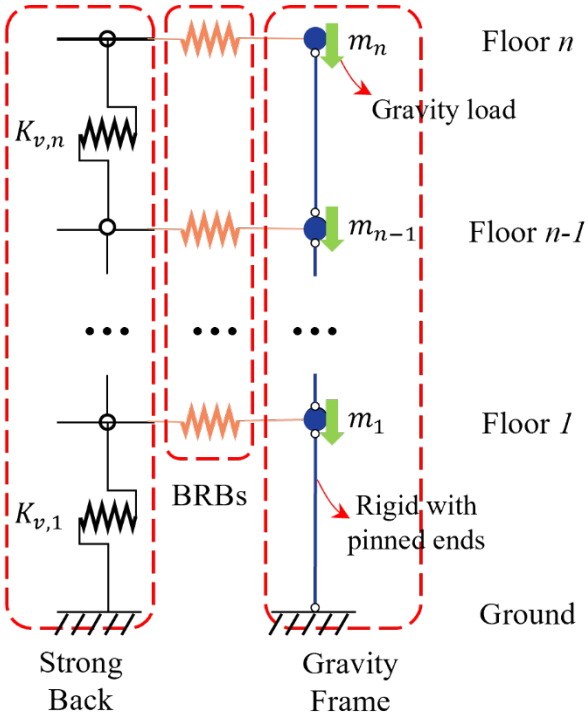

Figure 4 Numerical modeling of the SBDL system

As the strong back is intended to remain elastic, an elastic shear spring is used in each story to model the lateral inter-story deformation of the strong back, and the axial deformation of the strong back was assumed to be zero. For the determination of the stiffness of the elastic shear spring in the i^{th} story, it is calculated as the ratio of the yield lateral resistance of the strong back ($V_{y,i}$) to the yield lateral inter-story drift ($\delta_{y,i}$), i.e.,

$$K_{v,i} = \frac{V_{y,i}}{\delta_{y,i}} \tag{2}$$

The yield lateral resistance of the strong back is assumed to be equal to the force obtained by

assuming all BRBs have reached their capacities. The ratio of the expected capacity to the design yield resistance of BRBs is assumed to be 1.5 (Fahnestock et al., 2007; Zhao et al., 2011). The yield lateral inter-story drift of the i^{th} story can be calculated as

$$\delta_{y,i} = h_i \cdot \theta_{y,SB} \quad (3)$$

where h_i = the i^{th} story height and $\theta_{y,SB}$ = the yield inter-story drift ratio of the strong back. As different structures can be used as the strong back, e.g., steel braced frames, reinforced concrete shear walls, etc., and they have different typical yield inter-story drift ratios, a wide range of $\theta_{y,SB}$ will be considered in the following parametric study.

4 Optimization algorithm for $\boldsymbol{\Psi}$

As explained in Section 3, the key design parameter in the earthquake-resistant design of the SBDL system is the distribution of the total design lateral force to different floors, i.e., $\boldsymbol{\Psi}$. In this section, an optimization algorithm is developed to find the optimal $\boldsymbol{\Psi}$. The basic components underlying the developed optimization algorithm are elaborated as follows.

4.1 Nonlinear response history analyses (NRHAs)

The optimization approach used in this study is based on nonlinear response history analyses (NRHAs) of the structure subjected to a set of Maximum Considered Earthquakes (MCEs) with a return period of 2475 years (ASCE, 2016). In order to address the uncertainty in earthquake ground excitations, 22 ground motion (GM) records developed in FEMA P695 (FEMA, 2009) were adopted, which are considered sufficient to account for the variation in earthquake ground excitations. Table 2 provides basic information about the GM set. Additionally, the GM records were carefully selected to ensure their applicability to a range of structural systems and different sites, with more information available in FEMA P695 (FEMA, 2009). Following the scaling instructions, the GM records were scaled to match the seismic hazard of the prototype building specified in Section 3. The MCE spectrum and the response spectra of individual scaled GM records are presented in Figure 5.

220 **Table 2** Information on the ground motion record set (FEMA, 2009)

EQ ID No.	Earthquake			Recording Station	Source (Fault Type)
	M	Year	Name		
1	6.7	1994	Northridge	Beverly Hills - Mulhol	Thrust
2	6.7	1994	Northridge	Canyon Country-WLC	Thrust
3	7.1	1999	Duzce, Turkey	Bolu	Strike-slip
4	7.1	1999	Hector Mine	Hector	Strike-slip
5	6.5	1979	Imperial Valley	Delta	Strike-slip
6	6.5	1979	Imperial Valley	El Centro Array #11	Strike-slip
7	6.9	1995	Kobe, Japan	Nishi-Akashi	Strike-slip
8	6.9	1995	Kobe, Japan	Shin-Osaka	Strike-slip
9	7.5	1999	Kocaeli, Turkey	Duzce	Strike-slip
10	7.5	1999	Kocaeli, Turkey	Arcelik	Strike-slip
11	7.3	1992	Landers	Yermo Fire Station	Strike-slip
12	7.3	1992	Landers	Coolwater	Strike-slip
13	6.9	1989	Loma Prieta	Capitola	Strike-slip
14	6.9	1989	Loma Prieta	Gilroy Array #3	Strike-slip
15	7.4	1990	Manjil, Iran	Abbar	Strike-slip
16	6.5	1987	Superstition Hills	El Centro Imp. Co.	Strike-slip
17	6.5	1987	Superstition Hills	Poe Road (temp)	Strike-slip
18	7.0	1992	Cape Mendocino	Rio Dell Overpass	Thrust
19	7.6	1999	Chi-Chi, Taiwan	CHY101	Thrust
20	7.6	1999	Chi-Chi, Taiwan	TCU045	Thrust
21	6.6	1971	San Fernando	LA - Hollywood Stor	Thrust
22	6.5	1976	Friuli, Italy	Tolmezzo	Thrust

221

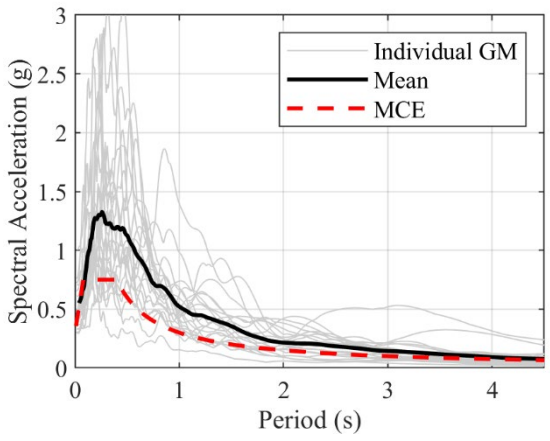

222

Figure 5 MCE spectrum and the response spectra of individual scaled GM records

4.2 Criteria and score for performance evaluation

Through the NRHA under GM *i*, the maximum absolute inter-story drift ratios of all stories can be extracted and represented by $\boldsymbol{\theta}_{max}^{i}$. Subsequently, the mean of $\boldsymbol{\theta}_{max}^{i}$ under the 22 GMs can be calculated as

$$\overline{\boldsymbol{\theta}}_{max} = \frac{\sum_{i=1}^{22} \boldsymbol{\theta}_{max}^{i}}{22} \tag{4}$$

For cases where the maximum absolute inter-story drift ratio at any story exceeded 10%, the results were excluded as the structure was considered to have collapsed.

For evaluation of the seismic response, two aspects are considered based on $\overline{\boldsymbol{\theta}}_{max}$: (1) the magnitude of the maximum absolute inter-story drift ratios, and (2) the distribution of the max absolute inter-story drift ratios over the stories. The magnitude can be evaluated by the mean of all the components of $\overline{\boldsymbol{\theta}}_{max}$,

$$mean(\overline{\boldsymbol{\theta}}_{max}) = \frac{\sum_{i=1}^{n} \bar{\theta}_{max,i}}{n} \tag{5}$$

where n is the number of stories and $\bar{\theta}_{max,i}$ is the i^{th} component of the vector $\overline{\boldsymbol{\theta}}_{max}$.

For the distribution of the maximum absolute inter-story drift ratios over the stories, a uniformity index is developed as

$$unif(\overline{\boldsymbol{\theta}}_{max}) = \left\| \frac{\frac{\overline{\boldsymbol{\theta}}_{max}}{\left\|\overline{\boldsymbol{\theta}}_{max}\right\|_1} - \frac{1}{n}}{1 - \frac{1}{n}} \right\|_{\infty} \tag{6}$$

where $\| \quad \|_1$ and $\| \quad \|_{\infty}$ represent the L1-norm and ∞-norm of a vector, respectively. The value of $unif(\overline{\boldsymbol{\theta}}_{max})$ ranges from 0 to 1, with lower value indicating better distribution. For the case where all the components of $\overline{\boldsymbol{\theta}}_{max}$ are the same, which indicates the most uniform distribution, $unif(\overline{\boldsymbol{\theta}}_{max})$ takes the value of 0. For the opposite extreme case where only one component of $\overline{\boldsymbol{\theta}}_{max}$ is nonzero, which indicates that all the lateral deformation concentrates in

one story, $unif(\overline{\boldsymbol{\theta}}_{max})$ takes the value of 1.

To account for both the magnitude and distribution of the maximum absolute inter-story drift ratios, a final performance score, η, is defined as

$$\eta = \alpha_1 \cdot mean(\overline{\boldsymbol{\theta}}_{max}) + \alpha_2 \cdot unif(\overline{\boldsymbol{\theta}}_{max}) \quad (7)$$

where α_1 and α_2 are weight factors for the magnitude and distribution, respectively. A lower value of η indicates a better overall performance. As the value of $mean(\overline{\boldsymbol{\theta}}_{max})$ is found to be in the range of [0, 0.02] in general and the value of $unif(\overline{\boldsymbol{\theta}}_{max})$ is in the range of [0,1], α_1 was taken as 50 and α_2 was taken as 1 in this study so that the contributions of the two aspects to the final performance score are on a comparable scale.

However, it is noted that the optimization of the design parameter in this study solely focuses on the magnitude and distribution of inter-story drift responses under strong earthquakes. The optimal design parameters obtained may differ if there are changes in the optimization criteria or the choice of ground motion records.

4.3 The optimization algorithm

An algorithm was developed to find the optimal $\boldsymbol{\Psi}$, as illustrated in Figure 6. The major steps include:

1. The starting $\boldsymbol{\Psi}$ is taken to have the same shape as the mass vector, and the SBDL system will be designed following the method specified in Section 3. The numerical model will be created accordingly and NRHAs will be conducted under 22 GMs. From the analysis under GM *i*, the maximum absolute inter-story drift ratios of all stories, $\boldsymbol{\theta}_{max}^{i}$, will be extracted. The mean results under the 22 GMs will be obtained following Eq. 4.

2. The magnitude and uniformity will be calculated following Eq. 5 and 6, respectively, based on which the final performance score η will be obtained following Eq. 7.

3. $\boldsymbol{\Psi}$ is updated based on the shape of $\overline{\boldsymbol{\theta}}_{max}$ in each iteration. This is because a large component of $\overline{\boldsymbol{\theta}}_{max}$ indicates the relative weakness of the corresponding story and implies the

need to strengthen that story to achieve a more uniform $\bar{\boldsymbol{\theta}}_{max}$. The update in each iteration follows

$$\boldsymbol{\Psi} = \frac{\boldsymbol{\Psi} + \Delta \frac{\bar{\boldsymbol{\theta}}_{max}}{\|\bar{\boldsymbol{\theta}}_{max}\|_1}}{\left\|\boldsymbol{\Psi} + \Delta \frac{\bar{\boldsymbol{\theta}}_{max}}{\|\bar{\boldsymbol{\theta}}_{max}\|_1}\right\|_1} \tag{8}$$

where Δ is the step size, and $\| \quad \|_1$ represent the L1-norm of a vector. The step size determines the amplitude of the change in $\boldsymbol{\Psi}$ in each iteration, which is taken as 0.05 in this study. The design of the SBDL system will be updated based on the updated $\boldsymbol{\Psi}$.

4. Steps 1 to 3 are repeated until the performance score η of one iteration is larger than that of the previous iteration. And the $\boldsymbol{\Psi}$ that resulted in the smallest η is taken as the optimal $\boldsymbol{\Psi}$.

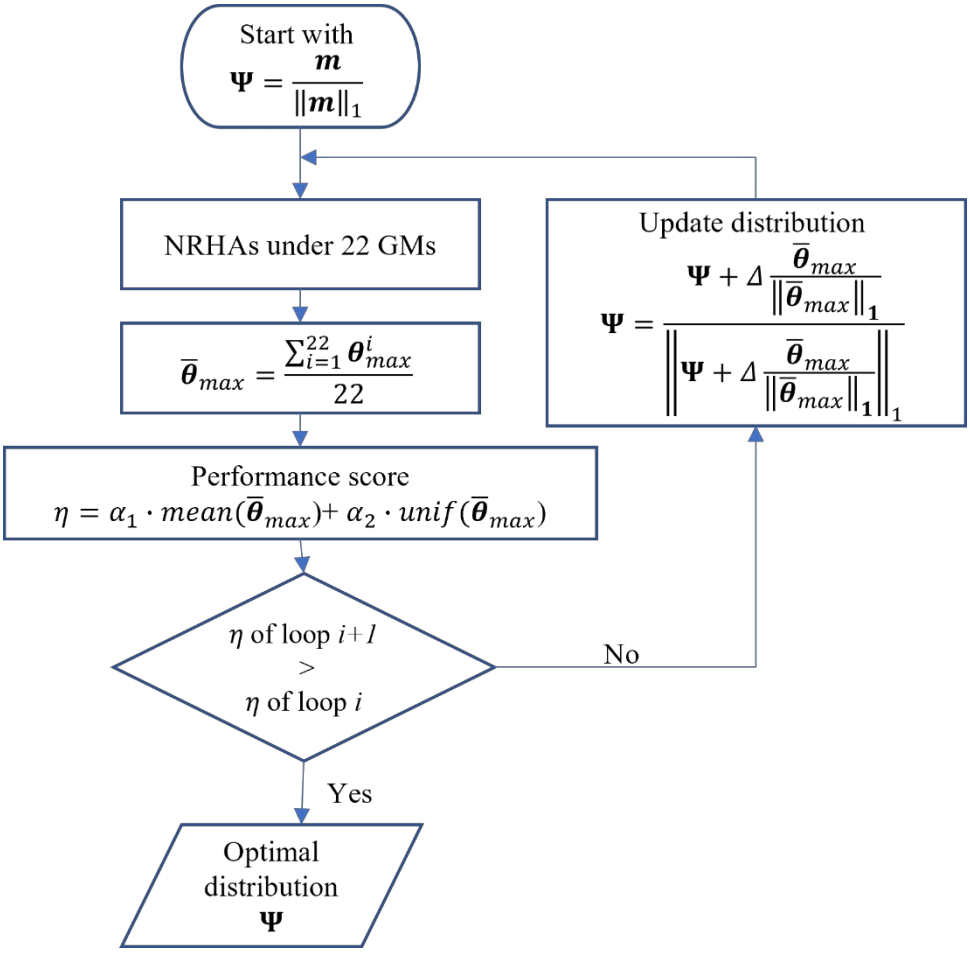

Figure 6 Flow of the algorithm to find the optimal $\boldsymbol{\Psi}$

4.4 Illustration of the optimization process by one example

To illustrate the iterative process searching for the optimal $\boldsymbol{\Psi}$, the process for one example case is presented in this section. The design details of the example case are as follows: the ratio of the total design lateral force to the total seismic weight ($\frac{V}{W}$) is 0.5; the yield inter-story drift ratio of the strong back ($\theta_{y,SB}$) is 0.1%; the damping ratio of the system (ξ) is 3%; the seismic mass is uniformly distributed over the height.

Figure 7 (a) and (b) show the evolution of $\boldsymbol{\Psi}$ and the resulted $\overline{\boldsymbol{\theta}}_{max}$ throughout the iterative optimization process, respectively. As shown, the starting $\boldsymbol{\Psi}$ took the shape of the mass distribution over the stories which is the vertical line in Figure 7(a). NRHAs were conducted under 22 GMs and the result $\overline{\boldsymbol{\theta}}_{max}$ was extracted. Then $\boldsymbol{\Psi}$ was updated following Eq. 8, and the process continued. In this case, 12 iterations in total were conducted, and the process stopped as the performance score η of 12th iteration is larger than η of 11th iteration. The $\boldsymbol{\Psi}$ of the 11th iteration was taken as the optimal $\boldsymbol{\Psi}$ for this example case which is shown by the thicker line in Figure 7.

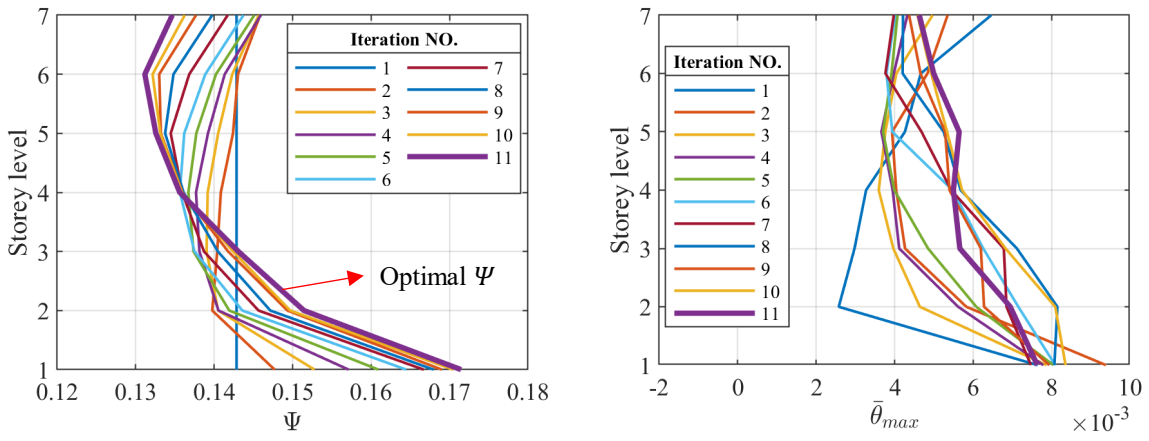

(a) (b)

Figure 7 The iterative optimization process for an example case: (a) $\boldsymbol{\Psi}$, (b) $\overline{\boldsymbol{\theta}}_{max}$

5 Parametric study and creation of database

A comprehensive parametric study was conducted for the SBDL system introduced in Section 3, in which 4 parameters are varied, namely, (1) the ratio of the total design lateral force to the total seismic weight ($\frac{V}{W}$), (2) the yield inter-story drift ratio of the strong back ($\theta_{y,SB}$),

295 (3) the damping ratio of the system (ξ), and (4) the distribution of the seismic mass over the
296 height. For each case in the parametric study, the optimal $\boldsymbol{\Psi}$ is obtained following the
297 optimization algorithm elaborated in Section 4. It is noted that the parametric study can be
298 expanded to cover the variation of more design parameters, for instance, the yield strength and
299 strain hardening rate of the steel of the BRB core plate.

300 For the ratio of the total design lateral force to the total seismic weight, $\frac{V}{W}$, five values
301 ranging from 0.3 to 0.8 with an interval of 0.1 were considered. In practice, the seismic mass
302 may not be uniformly distributed over the building's height. As such, in addition to the uniform
303 distribution, another three distributions as shown in Figure 8 were considered. Different
304 structures can be used as the strong back, e.g., steel braced frames, reinforced concrete shear
305 walls, etc. They have different typical yield inter-story drift ratios ($\theta_{y,SB}$). In this study, a wide
306 range of $\theta_{y,SB}$ from 0.1% to 1% with an interval of 0.1% were studied to reflect different
307 possible choices of the strong back. Moreover, different structures feature different levels of
308 damping. Five damping ratios ranging from 0.01 to 0.05 with an interval of 0.01 were examined.

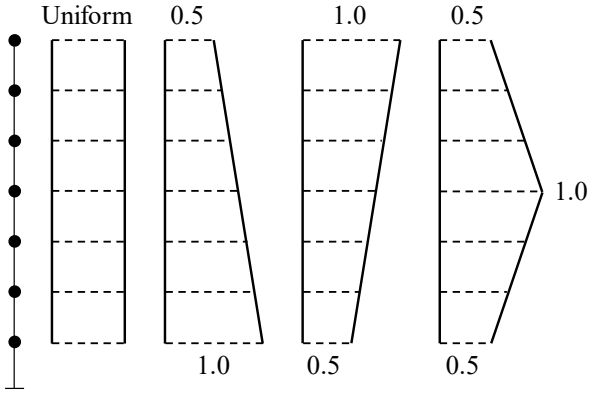

309

310 **Figure 8** Four mass distribution patterns considered in the parametric study

311 In total, 1200 cases were examined in the parametric study. A database consisting of 1200
312 samples was therefore created. A large variation exists in the optimal $\boldsymbol{\Psi}$s. For instance, Figure
313 9 shows the optimal $\boldsymbol{\Psi}$s of the 55 cases that have the uniform seismic mass distribution and the
314 $\frac{V}{W}$ of 0.5. Such variation is difficult to capture by conventional design methods, which

315 motivates the development of the AI-assisted method which will be elaborated on in the
316 following sections.

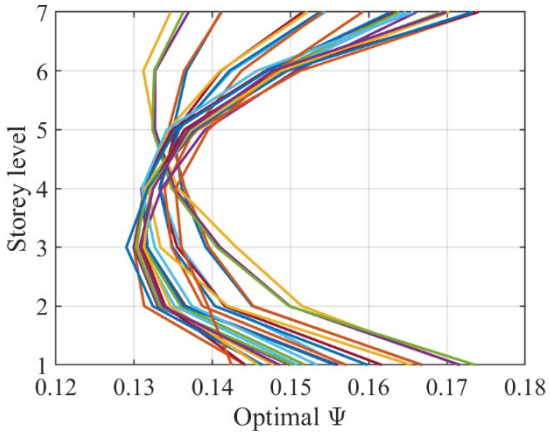

317

318 **Figure 9** Variation in optimal $\boldsymbol{\Psi}$s for cases with uniform mass distribution and $\frac{V}{W}$ of 0.5

319 **6 AI-assisted method to predict the optimal $\boldsymbol{\Psi}$**

320 In this section, an AI model, specifically, the multilayer perceptron artificial neural network
321 (referred to as the ANN model), is developed to predict the optimal $\boldsymbol{\Psi}$ based on the database
322 created through numerical simulation in the previous section. The features underlying the
323 development of the ANN model are elaborated in the following sections.

324 **6.1 Overview of the ANN model**

325 A neural network is a computational model that draws inspiration from biological neural
326 networks (Fausett, 2006). It is capable of adapting its predictions based on input data and
327 making generalizations. Within AI-based techniques, neural networks are the preferred method
328 for civil engineering applications due to their simplicity (Vanluchene & Sun, 1990; Messner et
329 al., 1994; Mitropoulou & Papadrakakis, 2011; Xiao et al., 2022; Wang & Chan, 2023). In this
330 study, we adopted the multilayer perceptron artificial neural network, which is one type of
331 neural network referred to as the ANN model. An ANN model consists of three types of layers
332 of neurons (also known as nodes): the input layer, hidden layer, and output layer, as depicted
333 in Figure 10. The number of nodes in the input layer is equal to the number of input features,

and the number of nodes in the output layer is equal to the number of output variables. In fully connected ANN models, each node in a layer is connected to all nodes in the next layer, with each connection represented mathematically by weight (w) and bias (b) parameters. The output of the i-th node in the hidden layer is given by:

$$h_i = s\left(\sum_{j=1}^{N} w_{ij}x_j + b_{ij}\right) \tag{9}$$

where $s()$ is called the activation function, N is the number of input nodes.

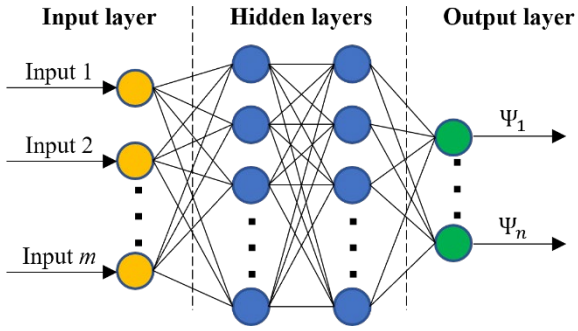

Figure 10 Illustration of the structure of an ANN model

After inputting an observation (or a *batch* of observations) into the network, a loss function is utilized to compare the predicted value to the actual value, a process known as forward propagation. Next, an algorithm moves "backward" through the network and determines the contribution of each parameter to the difference between the predicted and actual values, which is called backpropagation. At each propagation, the optimization algorithm decides how to adjust each weight to improve the output. To learn, neural networks repeat this cycle of forward propagation and backpropagation for each observation in the training data multiple times (each repetition is referred to as an *epoch*), steadily updating the parameter values.

6.2 Design of the ANN model

For this study, a fully connected ANN model with two hidden layers was adopted. The popular Python library *Keras* was used to build, train, and evaluate the ANN model (Chollet et al., 2015). The selection of input features plays a crucial role in the success of an ANN model. A large number of input features can slow the development and training of the model and

require a large amount of computer memory. Of greater significance is the fact that if irrelevant input features are incorporated into the model, the performance of the ANN may deteriorate. In this study, the knowledge-based input feature selection approach was adopted. Based on the knowledge of structural dynamics, design input features that can have an impact on the dynamic response of structures under strong earthquakes are used as the input features and they are listed in Table 3. The number of nodes in the input layer is set as the sum of the dimensions of all the input features. As the optimal $\boldsymbol{\Psi}$ is the target prediction, the number of nodes in the output layer was set as the dimension of $\boldsymbol{\Psi}$, i.e., the number of stories of the SBDL system. The *softmax* function was used as the activation function for the output layer nodes. The *softmax* activation function will make the output values be in the interval [0,1] and add up to 1, which conforms to the requirement for $\boldsymbol{\Psi}$. The activation function used for all the remaining nodes is the $ReLU$ function.

In order to prevent overfitting of the neural network, which occurs when the training error decreases but the test error increases, indicating poor generalization of the model, the early stopping technique was utilized. During the training process, the test (validation) loss was monitored at each epoch, and training was interrupted if the test loss did not improve after two epochs. In addition to this, hyperparameter optimization was performed for other parameters of the ANN model, and these optimal choices will be discussed in Section 6.4.

Table 3 Input features for the ANN model

Input features	Mass distribution ($\boldsymbol{m}$)
	Story height ($\boldsymbol{h}$)
	Total design lateral force (V)
	The yield inter-story drift ratio of the strong back ($\theta_{y,SB}$)
	Damping ratio (ξ)
	Yield strength of the BRB core plate steel
	Strain hardening rate of the BRB core plate steel

6.3 Train-test data split and data preprocessing

In order to assess the performance of the trained ANN models on unseen data, the database is first randomized and then divided into a training set (80% of the total data) and a test set (20% of the total data). The training set is exclusively used for the construction, optimization, and training of the ANN model, while the test set is kept separate until the final evaluation of the model.

Different input features may have varying scales and ranges. Without feature scaling, the ANN may be biased toward the features which have values higher in magnitude (Albon, 2018). As such, feature scaling is necessary to prevent bias towards features with higher magnitudes and ensure proportional contributions from each feature. Additionally, as the ANN uses gradient descent to optimize all the weights and biases, feature scaling can usually make the algorithm converge faster than without it (Ioffe & Christian, 2015). To achieve this, all input features in this study were scaled to the range [0,1] using the *MinMaxScaler* tool in the Python library scikit-learn (Pedregosa et al., 2011). To prevent data leakage, the scaler was only created using the training data and not any information outside the training set (Kaufman et al., 2012).

6.4 Hyperparameter optimization

In the context of an ANN model, hyperparameters refer to parameters that define the model's architecture, such as the number of neurons in each layer, the optimization algorithm, the number of epochs, the batch size, and so on. These hyperparameters must be optimized to ensure that the model can effectively solve the problem at hand. Hyperparameter optimization finds a set of hyperparameters that yields an optimal model which minimizes a predefined loss function on given data (Claesen & De Moor, 2015).

In this study, the grid search strategy was used to search for the optimal combination of hyperparameters. Four hyperparameters, namely, the type of optimization algorithm, the

number of neurons in each layer, the number of epochs and batch size, were varied. The spaces for each of the four hyperparameters are listed in Table 4. During the grid search, all possible combinations of the four hyperparameters were checked exhaustively. For each combination in the grid search, a 5-fold cross validation was conducted to evaluate the performance of the ANN as illustrated in Figure 11. For evaluation of the prediction accuracy, the metric of mean absolute percentage error (MAPE) was adopted.

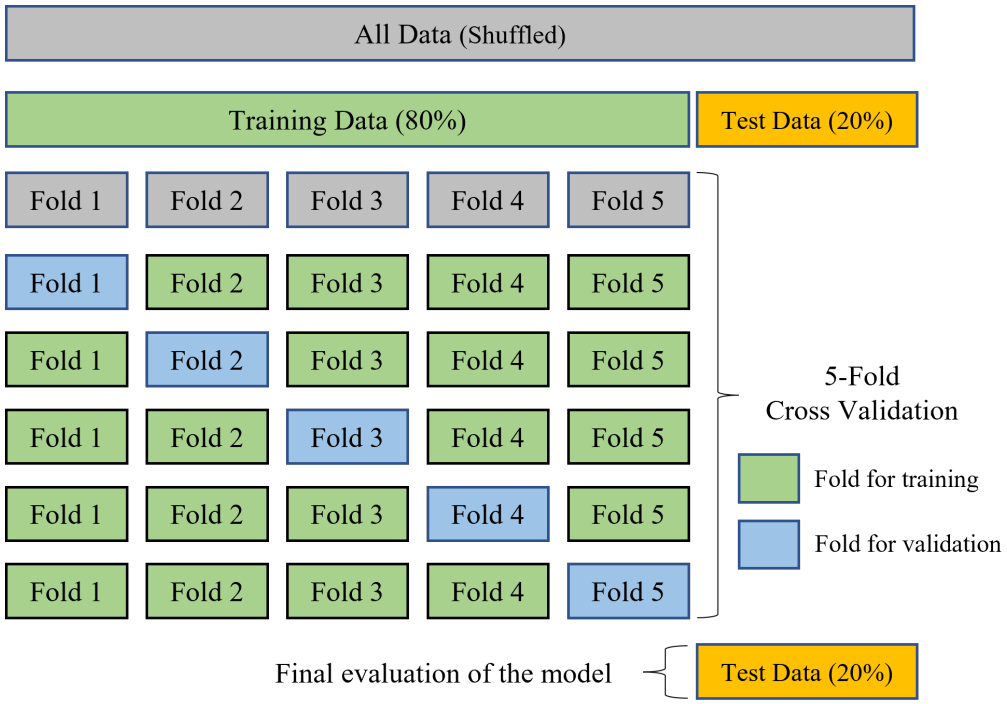

Figure 11 Five-fold cross validation adopted for hyperparameter optimization

Table 4 Hyperparameter space covered in the grid search

Hyperparameter	Space	Optimal choice
Optimization algorithm	'RMSprop', 'SGD', 'Adam'	'Adam'
Number of neurons in the two hidden layers	5, 10, 15, 20, 25	20
Number of epochs	25, 50, 75, 100, 125, 150	25
Batch size	1, 3, 5, 7, 9, 11	3

To implement the 5-fold cross-validated grid search, the technique combining the tools from two Python libraries (*Keras* and *scikit-learn*) was used as shown in Figure 12. Firstly, a function that returns a compiled ANN was created via *Keras*. Next the ANN model was wrapped using the tool *KerasRegressor* in scikit-learn. Subsequently, the cross-validated grid search tool *GridSearchCV* in scikit-learn was used to conduct the grid search and find the optimal hyperparameter combination. To illustrate the grid search for hyperparameter optimization, Figure 13 shows the MAPEs with both the number of epochs and batch size varying over their space. The combination of hyperparameters that resulted in the lowest MAPE was taken as the optimal one, which are listed in Table 4. The reliability of the selected hyperparameters was also validated by the performance of the constructed ANN model on data that had never been seen by the model (i.e., the test data), which will be provided in Section 6.6. However, the limitations and trade-offs of the grid-searching method need to be acknowledged and carefully considered. Specifically, the obtained hyperparameters may not be guaranteed to be the most optimal and may vary with different divisions of the training data. More hyperparameter optimization techniques are recommended to be explored in the future work to mitigate the limitations.

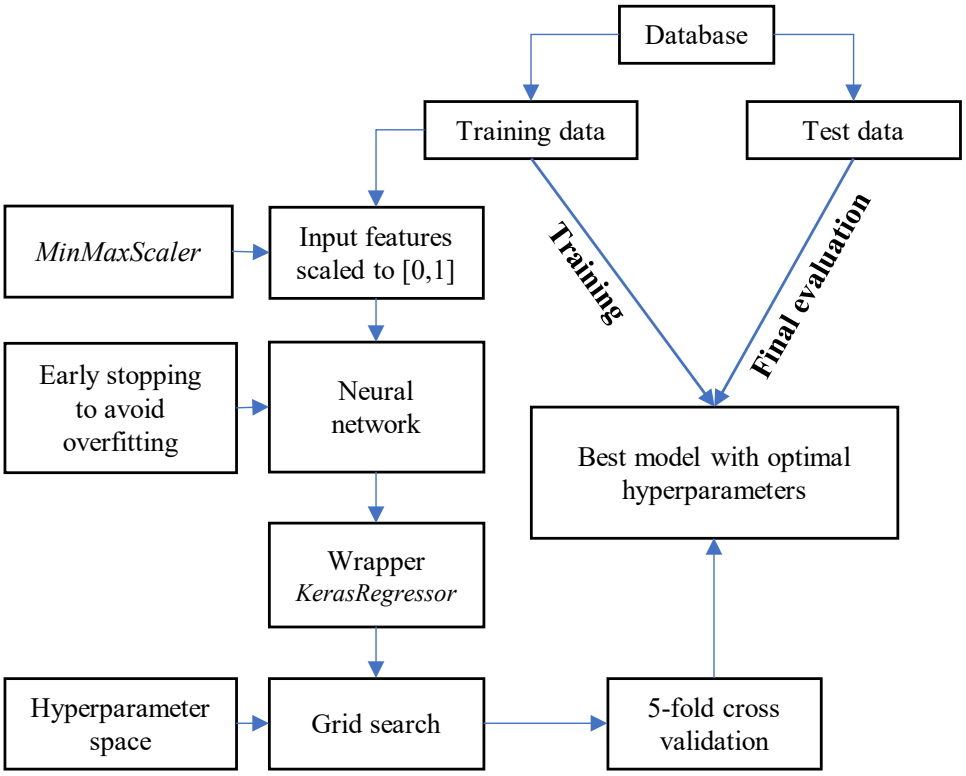

Figure 12 Procedure for building, hyperparameter optimization, training, and evaluation of the ANN model

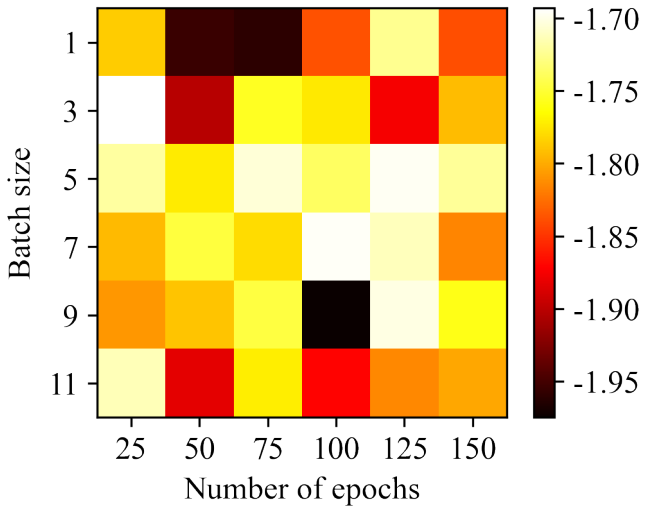

Figure 13 Effect of number of epochs and batch size on MAPE

6.5 Feature importance

In this study, the ANN model was trained to generate the optimized distribution of the design seismic load that can be directly utilized by structural designers. To investigate the significance of input variables in influencing the output of the ANN model, the importance of individual

features was quantified by using the permutation feature importance method. The permutation importance of a feature is defined as the decrease in a model performance score when the feature is randomly shuffled (Breiman, 2001). The shuffling of a feature breaks its relationship with the target variable, and the drop in the model score reflects the importance of that feature. The mean absolute percentage error was taken as the performance score. For the purpose of comparison, the obtained values were scaled by a common factor to ensure a sum of unity.

Figure 14 depicts the calculated feature importance values for each feature. As illustrated, the mass distribution at different floors emerges as a key determinant for the design base shear distribution, which aligns with conventional earthquake-resistant design principles. Notably, other design parameters, for example, the total design seismic load (V), the yield inter-story drift ratio of the strong back ($\theta_{y,SB}$), the damping ratio (ξ), also exhibit an impact on the output. This indicates an advantage of our proposed simulation-driven AI-assisted framework compared to conventional design method, as it allows for the consideration of more design input parameters in determining key design parameters.

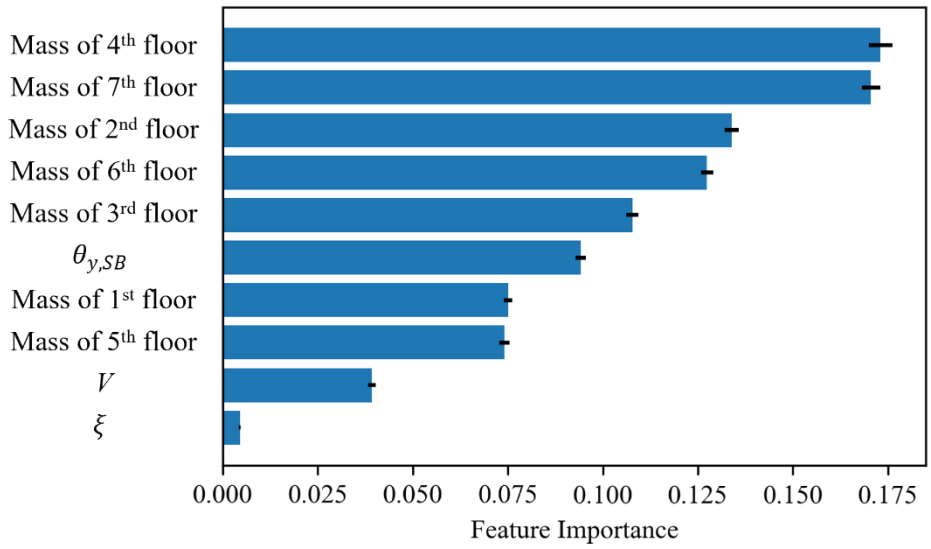

Figure 14 Feature importance of individual input features

6.6 Prediction and evaluation

After obtaining optimal hyperparameters, the ANN model was trained on the training set.

To evaluate the capability of the trained ANN to predict the optimal $\boldsymbol{\Psi}$, predictions were made for the cases in the test set, which have never been seen by the ANN model. A comparison between the predictions made by the ANN model and the true optimal $\boldsymbol{\Psi}$s was made, and Figure 15 shows the absolute errors and the statistical properties for all the cases in the test set. The two whiskers in the boxplot represent the 5th and 95th percentiles, respectively. As shown, the 95th percentiles at all stories are smaller than 0.01, which means the majority of the errors of the predicted $\boldsymbol{\Psi}$ from the optimal one is within 1% of the total design lateral force (i.e., $0.01V$).

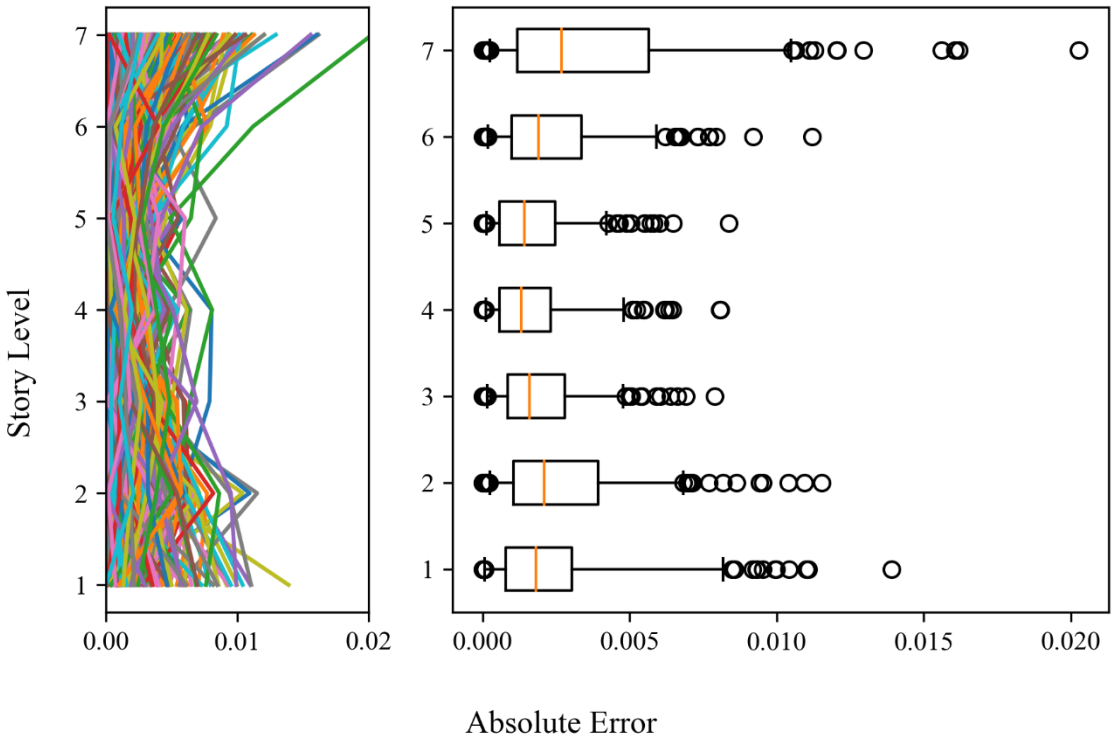

Figure 15 Absolute errors for all the cases in the test dataset (whiskers in the boxplot representing the 5th and 95th percentiles)

The results proved the capability of the ANN model to consider the effect of various design input parameters to obtain the optimal $\boldsymbol{\Psi}$ for earthquake-resistant design of the SBDL system, which validates the feasibility of the AI-assisted simulation-driven earthquake-resistant design framework. Moreover, this framework has the potential to be extended to cover more design

input parameters and other structural systems, which is an ongoing study by the authors.

7 Conclusions

In conventional earthquake-resistant design methods, a limited number of input factors and mainly elastic structural properties are considered in the determination of key design parameters. The design parameters determined in this way may not be the optimal ones. In this paper, an artificial intelligence (AI)-assisted simulation-driven earthquake-resistant design framework was developed.

This framework can automatically output optimal design parameters while considering nonlinear structural response under strong earthquakes and a large number of input factors. The primary innovation of the proposed framework lies in the fusion and integration of nonlinear numerical simulation and AI tools for earthquake-resistant design of building structures, marking a promising trend in this field.

~~The ultimate objective is to obtain optimal design parameters that take into account effects of various design input factors and the nonlinear response of the structure under strong earthquakes.~~ To illustrate the proposed framework, the determination of the height-wise distribution of the total design lateral force (denoted by $\boldsymbol{\Psi}$) for a strong back system is taken as an example. The essential components underlying the proposed framework and main findings are as follows:

1) A numerical model that can capture both the elastic and plastic properties of the structure was first developed for a strong back system with buckling-restrained braces, which enables the numerical simulation of the structural response under earthquake excitations.
2) An optimization algorithm was developed to find the optimal target design parameter, which is $\boldsymbol{\Psi}$. Two aspects, namely, the magnitude and the distribution of the maximum

lateral inter-story deformations, were taken into account for the performance evaluation. The optimization was based on the results of numerical nonlinear response history analyses subjected to 22 ground motion records.

3) A comprehensive parametric study was conducted in which a wide range of design input parameters were covered. For each case in the parametric study, the optimal $\boldsymbol{\Psi}$ was obtained following the developed optimization algorithm. A database of 1200 data points with each containing the design input information and the optimal $\boldsymbol{\Psi}$ was created.
4) An artificial neural network (ANN) model was created, optimized, and trained using the created database. The developed ANN model was proved to have a good capability to yield the optimal $\boldsymbol{\Psi}$ with the majority of the absolute errors within 1%, which validates the feasibility of the AI-assisted simulation-driven earthquake-resistant design framework.

It should be noted that this study focused on demonstrating the proposed framework using a single, relatively simple structural system. The database created for this study is relatively small in size, consisting of only 1200 samples, and the trained AI model only deals with the output of one key design parameter, namely the determination of the optimal $\boldsymbol{\Psi}$. As a result, the proposed framework may not be directly applicable for real-world practices. Further refinement of the framework is needed to make it suitable for realistic practices, which includes accurate and validated modeling of more complex structures, as well as consideration of additional design parameters. Moreover, while the study only utilized one AI method, investigating additional AI methods will provide further opportunities to leverage the power of AI.

Data availability

All data, models, and code that support the findings of this study are available from the corresponding author upon request. The database and the trained artificial neural network used

in this study will be available in the public domain on Github (*https://github.com/Nigel-7*).

Acknowledgement

This paper's research was funded by both the Chinese National Engineering Research Centre for Steel Construction (Hong Kong) and the Department of Civil and Environmental Engineering at The Hong Kong Polytechnic University through the Seed Funding. The support from the Guangdong Basic and Applied Basic Research Foundation (Grant No. 2021B1515020057 & 2023B1515040012) is also gratefully acknowledged.

References

Albon, C. (2018). Machine learning with python cookbook: Practical solutions from preprocessing to deep learning. " O'Reilly Media, Inc.".

American Society of Civil Engineers/Structural Engineering Institute (ASCE/SEI) 7-16. (2016). Minimum Design Loads and Associated Criteria for Buildings and Other Structures, Reston, Virginia, USA.

Anderson, J. C., Miranda, E., Bertero, V. V., and Kajima Research Team. (1991). "Evaluation of the seismic performance of a thirty-story RC building." UCB/EERC-91/16, Earthquake Engineering Research Centre, Univ. of California, Berkeley, Calif.

Breiman L. Random forests Machine learning 2001;45(1):5–32.

Brown, A. S., Yang, H. T., & Wrobleski, M. S. (2005). Improvement and assessment of neural networks for structural response prediction and control. Journal of Structural Engineering, 131(5), 848-850.

Calledda, C., Montisci, A., & Porcu, M. C. (2021). Optimal design of earthquake-resistant buildings based on neural network inversion. Applied Sciences, 11(10), 4654.

CEN. (2004). Eurocode 8: Design of structures for earthquake resistance. Part I: General rules, seismic actions and rules for buildings. EN 1998, European Committee for Standardization, Brussels.

Chao, S. H., Goel, S. C., & Lee, S. S. (2007). A seismic design lateral force distribution based on inelastic state of structures. Earthquake Spectra, 23(3), 547-569.

Chollet, F. & others. (2015). Keras. Available at: https://github.com/fchollet/keras.

Chopra, A. K. (2001). "Dynamics of structures: Theory and applications to earthquake engineering." 2nd Ed., Prentice-Hall, London.

Claesen, M., & De Moor, B. (2015). Hyperparameter search in machine learning. arXiv preprint arXiv:1502.02127.

Conte, J. P., Durrani, A. J., & Shelton, R. O. (1994). Seismic response modeling of multi-story buildings using neural networks. Journal of intelligent material systems and structures, 5(3),

392-402.

Fahnestock, L. A., Ricles, J. M., & Sause, R. (2007). Experimental evaluation of a large-scale buckling-restrained braced frame. Journal of structural engineering, 133(9), 1205-1214.

Fausett, L. V. (2006). Fundamentals of neural networks: architectures, algorithms and applications. Pearson Education.

FEMA. (2009). Quantification of building seismic performance factors. FEMA P695, Washington, DC.

GB 50011-2010. (2016). Code for seismic design of buildings, China Building Technology Research Institute. (in Chinese)

Hajirasouliha, I., & Moghaddam, H. (2009). New lateral force distribution for seismic design of structures. Journal of Structural Engineering, 135(8), 906-915.

Ioffe, Sergey; Christian Szegedy (2015). "Batch Normalization: Accelerating Deep Network Training by Reducing Internal Covariate Shift". arXiv:1502.03167 [cs.LG].

Jough, F. K. G., & Şensoy, S. (2016). Prediction of seismic collapse risk of steel moment frame mid-rise structures by meta-heuristic algorithms. Earthquake Engineering and Engineering Vibration, 15(4), 743-757.

Kassem, M. M., Nazri, F. M., Farsangi, E. N., & Ozturk, B. (2022a). Development of a uniform seismic vulnerability index framework for reinforced concrete building typology. Journal of Building Engineering, 47, 103838.

Kassem, M. M., Nazri, F. M., Farsangi, E. N., & Ozturk, B. (2022b). Improved vulnerability index methodology to quantify seismic risk and loss assessment in reinforced concrete buildings. Journal of Earthquake Engineering, 26(12), 6172-6207.

Kaufman, S., Rosset, S., Perlich, C., & Stitelman, O. (2012). Leakage in data mining: Formulation, detection, and avoidance. ACM Transactions on Knowledge Discovery from Data (TKDD), 6(4), 1-21.

Kiani, J., Camp, C., & Pezeshk, S. (2019). On the application of machine learning techniques to derive seismic fragility curves. Computers & Structures, 218, 108-122.

Lai, J.-W., & Mahin, S. A. (2015). Strongback System: A Way to Reduce Damage Concentration in Steel-Braced Frames. Journal of Structural Engineering, 141(9), 04014223.

Mazzoni, S., McKenna, F., Scott, M. H., and Fenves, G. L. (2006). OpenSees Command Language Manual. University of California, Berkeley, http://opensees.berkeley.edu/manuals/usermanual.

McKenna, F., Scott, M. H., and Fenves, G. L. (2010). “Nonlinear finite-element analysis software architecture using object composition.” Journal of Computing in Civil Engineering, 24(1):95-107.

Messner, J. I., Sanvido, V. E., & Kumara, S. R. (1994). StructNet: A neural network for structural system selection. Computer-Aided Civil and Infrastructure Engineering, 9(2), 109-118.

589 Mitropoulou, C. C., & Papadrakakis, M. (2011). Developing fragility curves based on neural
590 network IDA predictions. Engineering Structures, 33(12), 3409-3421.

591 Möller, O., Foschi, R. O., Quiroz, L. M., & Rubinstein, M. (2009). Structural optimization for
592 performance-based design in earthquake engineering: Applications of neural networks.
593 Structural safety, 31(6), 490-499.

594 National Research Council of Canada (NRCC). (2015). National Building Code of Canada,
595 13th ed., NBCC, Ottawa, ON, Canada.

596 Pedregosa, F., et al. (2011). Scikit-learn: Machine learning in Python. Journal of machine
597 Learning research, 12, 2825-2830.

598 Takeuchi, T., Chen, X., & Matsui, R. (2015). Seismic performance of controlled spine frames
599 with energy-dissipating members. Journal of Constructional Steel Research, 114, 51-65.

600 Tremblay, R. (2003). Achieving a Stable Inelastic Seismic Response for Multi-Story
601 Concentrically Braced Steel Frames. Engineering Journal, 40(2), 111-129.

602 Uniform Building Code (UBC). (1997). International Conference of Building Officials, Vol. 2,
603 California, US.

604 Wang, C., & Chan, T. M. (2023). Machine learning (ML) based models for predicting the
605 ultimate strength of rectangular concrete-filled steel tube (CFST) columns under eccentric
606 loading. Engineering Structures, 276, 115392.

607 Xiao, L., Li, Q. Y., Li, H., & Ren, Q. (2022). Loading capacity prediction and optimization of
608 cold-formed steel built-up section columns based on machine learning methods. Thin-Walled
609 Structures, 180, 109826.

610 Zhao, J., Li, Y., Wang, C., Chen, R., Yan, L., & Gong, C. (2021). Sliding corner gusset
611 connections in concentrically braced frames using BRBs: Numerical analysis and practical
612 design. Engineering Structures, 246, 113055.

613 Zhao, J., Wu, B., & Ou, J. (2011). A novel type of angle steel buckling-restrained brace: Cyclic
614 behavior and failure mechanism. Earthquake Engineering & Structural Dynamics, 40(10),
615 1083-1102.

616 Zhao, J., Yan, L., Wang, C., Zhou, Y., Chen, R., & Chan, T. M. (2023). Damage-control design
617 and hybrid tests of a full-scale two-story buckling-restrained braced steel moment frame with
618 sliding gusset connections. Engineering Structures, 275, 115263.

619 Zsarnoczay, A. (2013). Experimental and numerical investigation of buckling restrained braced
620 frames for Eurocode conform design procedure development. PhD Dissertation. Department
621 of Structural Engineering, Budapest University of Technology and Economics, Budapest.